Flexible array curvature and sound speed estimations with a maximum spatial lag-one coherence metric

Jiaxin Zhang[a], Kai Ding[b], and Muyinatu A. Lediju Bell[a,c,d]

[a]Department of Electrical and Computer Engineering, Johns Hopkins University, USA
[b]Department of Radiation Oncology and Molecular Radiation Sciences, Johns Hopkins Medicine, USA
[c]Department of Biomedical Engineering, Johns Hopkins University, USA
[d]Department of Computer Science, Johns Hopkins University, USA

ABSTRACT

Flexible transducer arrays have the potential to conform to various organ shapes and sizes during photoacoustic image-guided interventions. However, incorrect sound speeds and array shapes can interfere with photoacoustic target localization and degrade image quality. We propose a metric to estimate the sound speed surrounding a target and the radii of curvature of flexible arrays with approximately concave shapes. The metric is defined as the maximum lag-one spatial coherence of the time-delayed, zero-mean channel data received from a region of interest surrounding a photoacoustic target (which we abbreviate as mLOC). Performance is demonstrated with simulated and experimental phantom data. Three photoacoustic targets were simulated in k-Wave with 1540 m/s medium sound speed, and photoacoustic signals were received by a transducer with a flat shape and an 81.3 mm radius of curvature. To acquire experimental photoacoustic data with the flexible array placed on flat and curved surfaces, an optical fiber paired with a hollow metal needle was inserted into an 83-mm-radius hemispherical plastisol phantom at three locations. When implementing beamforming time delays to calculate mLOC, the associated sound speed and radii of curvature ranged 1080-2000 m/s and 60-120 mm, respectively. The sound speed and array curvature estimated by the maximized mLOC were 1540 m/s and 81 mm, respectively, in simulation, resulting in accuracies of 100% and 99.63%, respectively. The sound speed in the phantom was empirically estimated by the maximum of mLOC as 1543 m/s, which led to the array curvature estimation of 85 mm and the corresponding accuracy of 97.59%. Results demonstrate the potential of mLOC to approximate sound speeds and array radii when these variables are unknown in future flexible array imaging scenarios.

1. INTRODUCTION

Correct sound speed estimates and known element locations are two key components of accurate photoacoustic image reconstruction. Although sound speeds in the propagation media or tissue is typically unknown, a highly inaccurate sound speed can lead to degraded image quality,[1] with incorrect target depths[2] and sizes.[3] A flexible array transducer is particularly susceptible to these errors, as element positions are often unknown, which compounds with typical uncertainties regarding medium sound speeds.

We previously presented a flexible array for photoacoustic-guided interventions, which implemented delay-and-sum (DAS) beamforming in simulation and phantom studies,[4,5] and compared the image quality with that of a conventional linear transducer.[6] This work was based on known sound speeds and array curvatures. When array curvatures are unknown, possible solutions include deep neural networks[7] for transducer geometry parameter estimations, amplitude-based differentiable beamforming with a phase error loss,[8] or optimizing the average pixel brightness in a short-lag spatial coherence (SLSC) ultrasound.[9] Limitations of these approaches include requirements for multiple training examples, high computational complexity in differentiable volume reconstruction, and the multiple correlation calculations required to create SLSC images.

In this work, we propose to address challenges with array shape estimation by introducing a novel metric that calculates the maximum lag-one spatial coherence within a selected region of interest surrounding the photoacoustic target (i.e., mLOC). Training data and differential volume reconstruction are not necessary, and

only one coherence calculation is required per pixel location. As the accurate spatial coherence estimations depend on the correct sound speeds, which are required to delay the received channel data, mLOC can also be used to estimate the correct sound speed. It is likely that both sound speed and array curvature will be unknown. Therefore, a flat array can be employed to first use mLOC to estimate sound speed, followed by the estimation of the radius of curvature of a concave flexible array.

2. METHODS

2.1 mLOC Theory and Implementation

When accurate sound speed and transducer element positions are used in beamforming time delay calculations, signals associated with a photoacoustic target are expected to have higher spatial coherence than the surrounding background. However, if the sound speed is incorrect, the coherence-based curvature estimate will also be incorrect. Therefore, mLOC can first be used to estimate the sound speed of a radius with an infinite radius of curvature (i.e., an array that is approximately flat). Once sound speed is estimated with mLOC, the radius of curvature of the flexible array can then be determined with mLOC when an array is placed in a concave shape.

To calculate mLOC, correlation of delayed channel data received by equally spaced elements (i.e., spatial lags) was calculated when the flexible array was in either a flat or a curved shape,[4,5] resulting in a normalized spatial coherence function $\hat{R}$, as follows:[10]

$$\hat{R}(m) = \frac{1}{N-m} \sum_{i=1}^{N-m} \frac{\sum_{n=n_1}^{n_2} s_i(n) s_{i+m}(n)}{\sqrt{\sum_{n=n_1}^{n_2} s_i^2(n) \sum_{n=n_1}^{n_2} s_{i+m}^2(n)}} \tag{1}$$

where m is the spatial lag of one, $s_i(n)$ is the time-delayed, zero-mean photoacoustic signal received at the ith element from the nth depth (in samples), and N is the number of receive elements in the transducer (set to 128 for simulated data and limited to 80 for experimental data). The axial correlation kernel size (i.e., $n_2 - n_1$) was fixed to be approximately one wavelength. A 16 mm × 16 mm rectangular region of interest (ROI) was selected surrounding the target, and mLOC is reported as the maximum LOC within this ROI.

2.2 Simulation Setup

The k-Wave toolbox[11] was utilized to simulate a flexible array with 128 elements, 1 mm pitch, 5 MHz center frequency, and 20 MHz sampling frequency. The sound speed of the simulated medium was 1540 m/s. The photoacoustic targets within the medium were three round sources, each with a diameter of 0.6 mm. Two data acquisition cases were simulated. First, a flat array was placed on top of the medium, resulting in the photoacoustic sources located at a depth of 25 mm with lateral locations of -10 mm, 0 mm, and 10 mm relative to the transducer center. Second, a concave array with an 81.3 mm radius of curvature was simulated with the three acoustic sources placed at depths of 40 mm, 50 mm, and 60 mm and lateral locations of -10 mm, 0 mm, and 10 mm, respectively, relative to the transducer center.

2.3 Experimental Setup

To acquire photoacoustic data with the flexible array, a hemispherical phantom was constructed using plastisol (Bait Plastics, MO, USA). The phantom has a radius of curvature of 83 mm. The optical fiber was inserted into a 1.25 mm-diameter hollow metal needle. The optical fiber tip and the needle tip aligned and were used as the photoacoustic target. This optical fiber-needle pair was moved inside the phantom, parallel to the flat surface.

Experimental data were acquired using a flexible array (Japan Probe and Hitachi, Japan) with 128 elements, 0.8 mm element width, 1 mm element pitch, a center frequency of 5 MHz, and a sampling frequency of 20 MHz. The array was connected to a Vantage 128 ultrasound scanner (Verasonics Inc., WA, USA), which was synchronized with a Phocus Mobile laser (Opotek, Inc., Carlsbad, CA, USA) emitting at the wavelength of 750 nm through an optical fiber with a 600 um core diameter. The average laser energy measured at the optical fiber tip was 1.72 mJ.

Similar to the simulation setup, experimental data were acquired in two setup cases, as illustrated in Fig. 1. First, the flexible array was placed on top of the flat surface of the hemispherical phantom. The tip of the optical
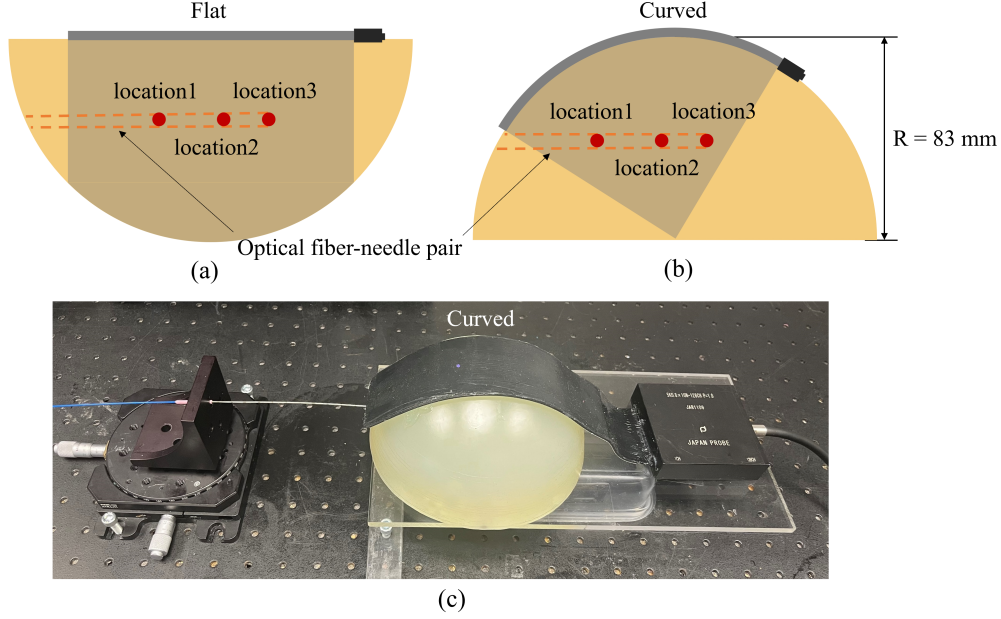
Figure 1. Schematic diagrams of the experimental setup with the flexible array placed on (a) flat and (b) curved surfaces of a hemispherical phantom, with the image field-of-view shown in gray. (c) Photograph of the flexible array conforming to the hemispherical surface of the experimental phantom.

fiber-needle pair, or the photoacoustic target, was imaged at three locations with the same depth, as shown in Fig. 1(a). Second (Figs. 1(b) and (c)), the flexible array was placed on the curved surface of the phantom, and the optical fiber-needle pair was moved inside the phantom along the same path as that in the first case. The photoacoustic data were acquired at three locations. At each target location in both cases, 20 photoacoustic images were acquired.

2.4 Sound Speed and Array Radius Estimations

A radius of 10^6 mm was utilized to calculate the transducer element positions of an approximately flat array with the time-delay equation previously derived for a concave curvature.[5] The mLOC was then plotted as a function of sound speeds ranging 1080-2000 m/s (i.e., 1540 ± 460 m/s, which is equivalent to $\pm 30\%$ deviation from 1540 m/s) with 10 m/s increments. When implemented with the experimental data, the mean mLOC of 20 frames was calculated with each sound speed increment. The average sound speed of the maximum of these plots for each photoacoustic target was the estimated sound speed. The simulated estimates were compared to ground truth simulation values to determine accuracy.

To estimate array radius of curvature required for time delay calculations (i.e., R_{delay}), the estimated sound speed determined by the flat array was fixed, and mLOC was then plotted as a function of R_{delay} ranging 60-120 mm with 1 mm increments. When implemented with the experimental data, the mean mLOC of 20 frames was calculated with each R_{delay} increment. The average R_{delay} of the maximum of these plots for each photoacoustic target was the estimated array radius. These estimates were compared to ground truth values to determine accuracy.

To provide additional confirmation of the accuracy of the estimated sound speed and R_{delay}, SLSC beamforming[10, 12, 13] was implemented to display resulting images. The spatial coherence function in Eq. 1 was employed with $M = 3$ for photoacoustic data and $M = 6$ for ultrasound data. The values for each axial and lateral SLSC pixel location were obtained using the following equation:

$$R_{sl} = \int_{m=1}^{M} \hat{R}(m) dm \approx \sum_{m=1}^{M} \hat{R}(m) \qquad (2)$$

To show the relative locations of the three targets in a single photoacoustic image, one example channel data acquisition from each target was beamformed and normalized to the brightest pixel within the beamformed image, then the three normalized images were summed (i.e., compounded) to create a single image.

3. RESULTS

The first row of Fig. 2 presents the mLOC plots obtained from simulated data. Fig. 2(a) shows mLOC as a function of sound speed with the flexible array in a flat shape. There is an alignment of the plots obtained with the three photoacoustic targets located at different lateral locations. The maximum value of each plot is obtained at the sound speed of 1540 m/s, which is the same as the ground truth sound speed, yielding 100% sound speed estimation accuracy. Fig. 2(b) shows mLOC as a function of R_{delay} with the flexible array in a concave shape and the sound speed fixed at the estimated 1540 m/s. Maximum values of each plot were obtained at the R_{delay} values of 80 mm, 82 mm, and 81 mm for target locations 1, 2, and 3, respectively, with an average R_{delay} of 81 mm, resulting in an estimation of curvature of 99.63% relative to the 81.3 mm ground truth radius of curvature.

The second row in Fig. 2 shows the mLOC curves obtained from experimental data. Fig. 2(c) shows mLOC as a function of sound speed with the flexible array on the flat surface of the hemispherical phantom. The maximum value of each plot is obtained at the sound speeds of 1550 m/s, 1560 m/s, and 1520 m/s for locations 1, 2, and 3, respectively, resulting in an average estimated sound speed of 1543 m/s. Fig. 2(d) shows the mean ± standard deviation mLOC as a function of R_{delay} with the flexible array placed on the curved surface of the phantom and the sound speed fixed at 1543 m/s. The maximum of the mean values were obtained at R_{delay} values of 77 mm, 84 mm, and 94 mm, resulting in an average of 85 mm for the estimated array curvature and an estimation accuracy of 97.59% (relative to the ground truth radius of 83 mm).

Fig. 3 shows an SLSC photoacoustic image overlaid on the SLSC ultrasound image, both created with the estimated sound speed (1543 m/s) and array curvature (85 mm) and acquired with the flexible array on the
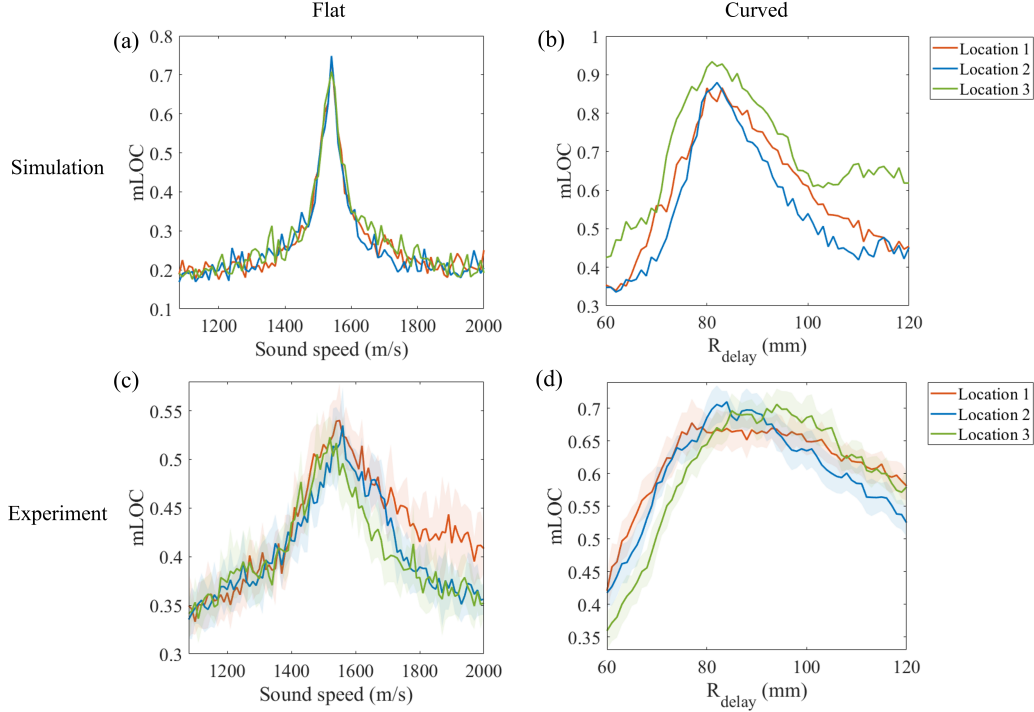

Figure 2. (a,b) Simulated and (c,d) experimental mLOC results as a function of (a,c) sound speed and (b,d) R_{delay}, with the flexible array in flat and curved shapes, respectively. The solid lines and shaded colors in (c) and (d) show the means and standard deviations of the 20 experimental channel data frames.
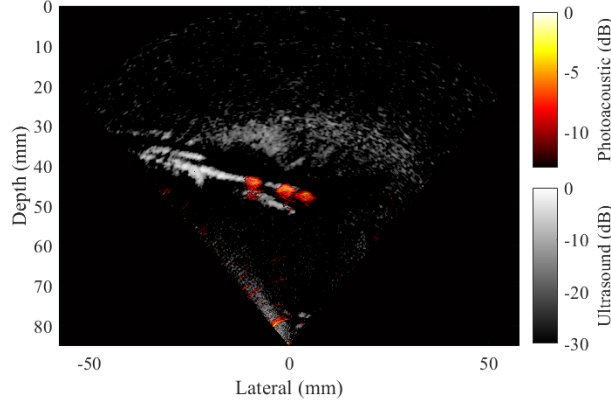
Figure 3. Example compounded photoacoustic SLSC image ($M = 3$) of the photoacoustic target appearance at three separate locations, overlaid on ultrasound SLSC image ($M = 6$) of the needle. The photoacoustic and ultrasound images are displayed with a 13 dB and 30 dB dynamic range, respectively.

curved phantom surface. The photoacoustic target (i.e., the tip of the optical tip-needle pair) at the three locations can be visualized as the high-coherence regions in the photoacoustic image. The metal needle can be distinguished from the background plastisol, based on its high coherence in the corresponding ultrasound image. Note that the field-of-view shown in Fig. 3 is rotated relative to the field-of-view illustrated in Fig. 1(b), resulting in the needle path shown at an oblique angle and the three locations shown at different depths in the reconstructed image.

4. DISCUSSION

This work is the first to demonstrate that the proposed mLOC metric can be used to estimate sound speed and radius of curvature. With the flexible array in a flat shape, sound speed was iterated and mLOC was plotted as a function of the iterated sound speeds, then the average of the sound speeds obtained at peak mLOC values was reported as the estimated sound speed. Following this estimation, the transducer was placed in a concave shape, the radius of curvature implemented in time-delay calculations was iterated, and mLOC was plotted as a function of the iterated radii. Array curvature was then estimated as the average of radii obtained at the maximum mLOC values for each of the photoacoustic targets. The estimation accuracies of 99.63% and 97.59% in simulation and phantom experiment, respectively, indicate the feasibility of the proposed method. In addition, SLSC ultrasound and photoacoustic images presented in Section 3 show good visibility of the target at the three locations along the needle path, demonstrating that the proposed mLOC metric is produces sound speed and array radius that are suitable to reconstruct interpretable images.

Although the actual sound speed of the plastisol phantom was not empirically measured, the simulation results share similar trends to the experimental results (e.g., the alignment of multiple mLOC curves as a function of sound speed). The effectiveness and accuracy of the experimental sound speed estimation could be verified in the future by measuring the SoS in the plastisol phantom using techniques such as the pulse-echo transmit-receive method[14] or a specialized sound speed measurement cell.[15] In addition, the sound speed estimation method can be applied not only to the flexible array, but also to other ultrasound transducers, as long as the transducer element positions are known. Future work can include demonstrations of the generalization of the proposed method for sound speed estimation using different types of transducers and media surrounding photoacoustic targets of interest.

5. CONCLUSION

A novel spatial coherence-based metric named mLOC for sound speed estimation and flexible array radius estimation in photoacoustic imaging was presented. Simulation results demonstrate that the mLOC metric

successfully estimated sound speed with a flat flexible array and array curvature with a concave flexible array. Experimental results produced 97.59% array radius estimation accuracy and interpretable photoacoustic and ultrasound SLSC images formed with the estimated parameters. Results demonstrate that the proposed mLOC metric is promising to improve image quality and target localization for photoacoustic-guided surgeries and interventions that employ flexible array geometries.

ACKNOWLEDGMENTS

REFERENCES

[1] Cong, B., Kondo, K., Namita, T., Yamakawa, M., and Shiina, T., "Photoacoustic image quality enhancement by estimating mean sound speed based on optimum focusing," *Japanese Journal of Applied Physics* **54**(7S1), 07HC13 (2015).

[2] Chen, Q. and Zagzebski, J. A., "Simulation study of effects of speed of sound and attenuation on ultrasound lateral resolution," *Ultrasound in medicine & biology* **30**(10), 1297–1306 (2004).

[3] Mori, S., Kanai, H., and Arakawa, M., "Speed-of-sound estimation in ultrasound propagation medium by considering size of target scatterer," *Journal of Medical Ultrasonics* **50**(2), 151–165 (2023).

[4] Zhang, J., Wiacek, A., González, E., Feng, Z., Ding, K., and Bell, M. A. L., "A flexible array transducer for photoacoustic-guided surgery," in [*2022 IEEE International Ultrasonics Symposium (IUS)*], 1–4, IEEE (2022).

[5] Zhang, J., Wiacek, A., Feng, Z., Ding, K., and Bell, M. A. L., "Flexible array transducer for photoacoustic-guided interventions: phantom and ex vivo demonstrations," *Biomedical Optics Express* **14**(8), 4349–4368 (2023).

[6] Zhang, J., Wiacek, A., Feng, Z., Ding, K., and Bell, M. A. L., "Comparison of flexible array with laparoscopic transducer for photoacoustic-guided surgery," in [*Photons Plus Ultrasound: Imaging and Sensing 2023*], **12379**, 205–212, SPIE (2023).

[7] Noda, T., Azuma, T., Ohtake, Y., Sakuma, I., and Tomii, N., "Ultrasound imaging with a flexible probe based on element array geometry estimation using deep neural network," *IEEE Transactions on Ultrasonics, Ferroelectrics, and Frequency Control* **69**(12), 3232–3242 (2022).

[8] Hyun, D., Narayan, S. V., Simson, W., Zhuang, L. L., and Dahl, J. J., "Flexible array shape estimation using differentiable beamforming," in [*2023 IEEE International Ultrasonics Symposium (IUS)*], 1–4, IEEE (2023).

[9] Omidvar, A., Rohling, R., Cretu, E., Cresswell, M., and Hodgson, A. J., "Shape estimation of flexible ultrasound arrays using spatial coherence: A preliminary study," *Ultrasonics* **136**, 107171 (2024).

[10] Lediju, M. A., Trahey, G. E., Byram, B. C., and Dahl, J. J., "Short-lag spatial coherence of backscattered echoes: Imaging characteristics," *IEEE transactions on ultrasonics, ferroelectrics, and frequency control* **58**(7), 1377–1388 (2011).

[11] Treeby, B. E. and Cox, B. T., "k-wave: Matlab toolbox for the simulation and reconstruction of photoacoustic wave fields," *Journal of Biomedical Optics* **15**(2), 021314–021314 (2010).

[12] Bell, M. A. L., Kuo, N., Song, D. Y., and Boctor, E. M., "Short-lag spatial coherence beamforming of photoacoustic images for enhanced visualization of prostate brachytherapy seeds," *Biomedical optics express* **4**(10), 1964–1977 (2013).

[13] Graham, M. T. and Bell, M. A. L., "Photoacoustic spatial coherence theory and applications to coherence-based image contrast and resolution," *IEEE Transactions on Ultrasonics, Ferroelectrics, and Frequency Control* **67**(10), 2069–2084 (2020).

[14] Madsen, E. L., Dong, F., Frank, G. R., Garra, B. S., Wear, K. A., Wilson, T., Zagzebski, J. A., Miller, H. L., Shung, K. K., Wang, S., et al., "Interlaboratory comparison of ultrasonic backscatter, attenuation, and speed measurements.," *Journal of ultrasound in medicine* **18**(9), 615–631 (1999).

[15] Fortin, T. J., Laesecke, A., Freund, M., and Outcalt, S., "Advanced calibration, adjustment, and operation of a density and sound speed analyzer," *The Journal of Chemical Thermodynamics* **57**, 276–285 (2013).